PAPER • OPEN ACCESS

Cryogenic $^9\text{Be}^+$ Penning trap for precision measurements with (anti-)protons

View the article online for updates and enhancements.

Cryogenic ^{9}Be$^+$ Penning trap for precision measurements with (anti-)protons

M Niemann[1,2] , **T Meiners**[1,2] , **J Mielke**[1,2] , **M J Borchert**[1,3], **J M Cornejo**[1,2],
S Ulmer[3] **and C Ospelkaus**[1,2,4]

[1] Insitut für Quantenoptik, Leibniz Universität Hannover, Welfengarten 1, 30167 Hannover, Germany
[2] Laboratorium für Nano- und Quantenengineering, Leibniz Universität Hannover, Schneiderberg 39, 30167, Hannover, Germany
[3] Ulmer Fundamental Symmetries Laboratory, RIKEN, Wako, Saitama 351-0198, Japan
[4] Physikalisch-Technische Bundesanstalt Braunschweig, Bundesallee 100, 38116 Braunschweig, Germany

E-mail: christian.ospelkaus@iqo.uni-hannover.de

Abstract

Cooling and detection schemes using laser cooling and methods of quantum logic can contribute to high precision CPT symmetry tests in the baryonic sector. This work introduces an experiment to sympathetically cool protons and antiprotons using the Coulomb interaction with a ^{9}Be$^+$ ion trapped in a nearby but separate potential well. We have designed and set up an apparatus to show such coupling between two identical ions for the first time in a Penning trap. In this paper, we present evidence for successful loading and Doppler cooling of clouds and single ions. Our coupling scheme has applications in a range of high-precision measurements in Penning traps and has the potential to substantially improve motional control in these experiments.

Keywords: Penning trap, laser cooling, trapped ions, g-factor, proton, antiproton, CPT invariance

(Some figures may appear in colour only in the online journal)

1. Introduction

Precise comparisons of the fundamental properties of matter/antimatter conjugates on the single particle level provide sensitive tests of CPT symmetry and the associated Lorentz symmetry in the Standard Model of Particle Physics [1, 2]. Important examples for this are comparisons of charge-to-mass ratios and magnetic moments of antiprotons and protons in Penning traps, where much experimental progress has been made recently [3–6]. However, especially in case of the most precise magnetic moment measurements [5], which rely on the double Penning trap technique [7], the efforts are impeded

by the absence of fast and deterministic preparation schemes for the motional state of the particle. Standard laser-based manipulation and cooling techniques well established in atomic physics cannot be applied directly to a single proton or antiproton, as the nuclear spin is their only internal degree of freedom. Therefore, current state of the art experiments apply sub-thermal resistive cooling methods, where the particle is coupled to cryogenic resistors [8]. These time-consuming procedures are ultimately required to prepare particles with motional temperatures at the level of $T \leqslant 0.15$ K [9], which is essential for the high-fidelity spin state detection carried out in these experiments. In our currently most precise experiments [5], the sub-thermal cooling process constitutes the biggest time contribution in the measurement scheme, about 25 min per cooling attempt to prepare a particle cold enough for g-factor measurements. Therefore, such experiments would considerably profit from the development of laser-cooling

schemes, which deterministically provide particles at mode-temperatures below the single-spin-state detection threshold within much reduced time. This is the inspiration and motivation to implement methods to sympathetically cool protons and antiprotons by coupling them to a co-trapped 'logic' ion that can be manipulated. Laser-cooling of the 'logic'-ion and subsequent mode energy transfer will provide deterministically cold protons/antiprotons on time-scales of seconds. This will outperform the currently used methods due to considerably improved sampling statistics and the lower particle energies achieved, which will also further reduce systematic uncertainties. In future experiments, quantum logic inspired manipulation techniques could also be applied for state readout. Moreover, any techniques developed to mitigate this could well be extended to other charged particles that are difficult to manipulate directly, for example to highly charged ions for ultra-stringent tests of bound state quantum electrodynamics. Different coupling schemes have been proposed [10, 11] and are being worked on [12–17]. This article describes the necessary steps to apply sympathetic cooling of protons and antiprotons via direct Coulomb coupling in an advanced Penning trap system. Towards this end, we demonstrate operation of a cryogenic $^9\mathrm{Be}^+$ Penning trap which supplies the laser cooled ions for sympathetic cooling and quantum logic spectroscopy.

2. Coupling concept

For charged particles, the Coulomb interaction provides the strongest coupling between particles and makes a natural choice for sympathetic cooling and state transfer. Proposals to exploit this idea for sympathetic cooling and state detection have been made using different approaches, namely trapping the particles in a common potential well [18, 19], a shared-electrode-approach [10] and a free-space approach where the ions are located in separate potential wells [11]. As particles of opposite charge cannot be trapped in a common electrostatic potential well, we pursue the direct coupling approach in order to be able to address negatively charged particles as well. This approach has been successfully demonstrated in radio-frequency surface traps for particles of equal charge-to-mass ratio [12, 13].

In a Penning trap, charged particles are trapped by superimposing a strong magnetic field along the z-direction with a static electric quadrupole field confining the motion along that axis. The resulting motion can be described by three modes: a harmonic oscillation with frequency ν_z along the z-axis called the axial mode and two radial modes called magnetron and modified cyclotron modes with frequencies ν_- and ν_+ [20].

For two charged particles with charges $q_{1,2}$ trapped in separate harmonic potential wells along the z-axis with their equilibrium positions separated by d_0 and displacements $z_{1,2}$ from their respective equilibrium positions, the Coulomb interaction is described by the potential

$$U(z_1, z_2) = \frac{1}{4\pi\varepsilon_0} \frac{q_1 q_2}{d_0 - (z_1 - z_2)}, \qquad (1)$$

where ε_0 is the vacuum permittivity. Following the lines of [12] and using the standard ladder operators a_i and $a_i^\dagger$, the first order interaction can be expressed as

$$\frac{q_1 q_2}{2\pi\varepsilon_0 d_0^3} (z_1 z_2) \approx \hbar \Omega_{\mathrm{ex}} \left(a_1 a_2^\dagger + a_1^\dagger a_2 \right), \qquad (2)$$

where the last step assumes the angular frequencies ω_1 and ω_2 being close to each other. Here,

$$\Omega_{\mathrm{ex}} = \frac{q_1 q_2}{4\pi\varepsilon_0 d_0^3 \sqrt{m_1 m_2}\sqrt{\omega_1 \omega_2}} \qquad (3)$$

is the coupling rate, m_1, m_2 denote the respective masses of the particles and $\hbar$ is the reduced Planck constant. For resonant (identical) trap frequencies $\omega_1 = \omega_2 = \omega_0$, the oscillators 1 and 2 swap energies with a period of $2\tau_{\mathrm{ex}}$, and exchange time $\tau_{\mathrm{ex}} = \pi/(2\Omega_{\mathrm{ex}})$.

For given particles, the coupling rate (3) scales strongly with the interparticle distance d_0, and to a lesser extent with the axial trap frequencies $\omega_{1,2}$. It would be favorable to combine low motional frequencies with a small distance between potential wells, but as decreasing the length scale of a two-well potential increases the gradient and curvature of the potential, the motional frequencies will scale unfavorably. Due to the scaling of Ω_{ex} with d_0^{-3} and ω_0^{-1}, a system with small length scales and a tighter confinement is desirable. This will ultimately demand for a miniaturised Penning trap, which is currently under development. The version of the Penning trap which is installed for the first demonstration experiments presented in this manuscript is shown in figure 1. To observe the coupling, a procedure similar to [12] could be used. In order to achieve a stable coupling rate during the energy exchange periods (tens of milliseconds), axial frequency fluctuations should be small compared to the coupling rate (several or several tens of Hz). This requires relative voltage stabilities on the order of 10^{-5}; in our current precision experiments we reach about 500-fold higher axial frequency stabilities. The exchange times are fast compared to the expected ultra-low heating rates [8] in our cryogenic Penning trap system.
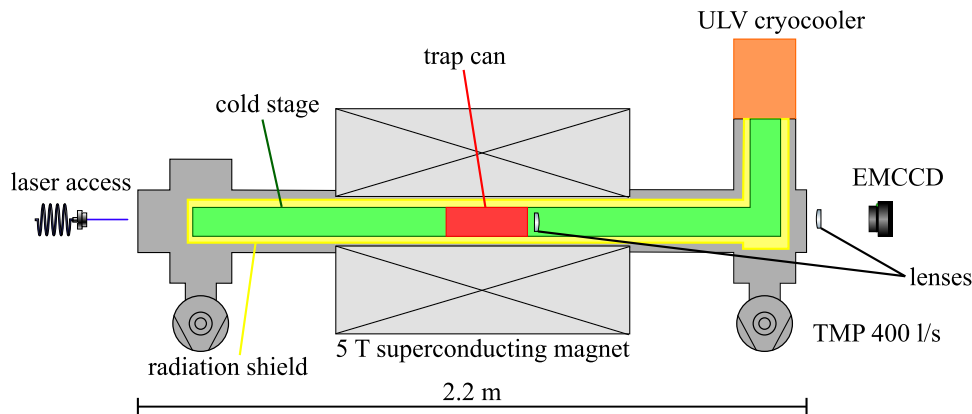
3. Experimental setup

The design of the experimental apparatus follows constraints defined by the apparatus of the BASE experiment, located at the antiproton decelerator of CERN [15]. This ensures mechanical compatibility of our system with the facilities at CERN to allow applying the demonstrated techniques on antiprotons in the future.

3.1. Superconducting magnet

The magnetic field for trapping ions is supplied by a high homogeneity wet superconducting magnet supplied by *Oxford Instruments* identical to the one described in [15], but operated at a higher magnetic field of $B_0 = 5\,\mathrm{T}$. The experiment is placed in the horizontal room temperature bore. The magnet's characterization results were in line with the data in [15] with
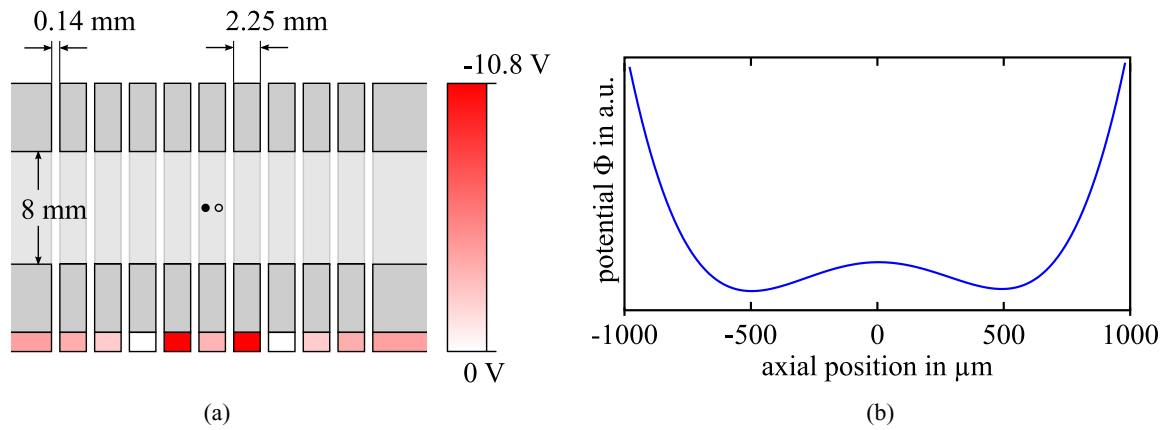
Figure 1. (a) Cut view of the cylindrical Penning trap for coupling of axial motional degrees of freedom. The applied trap voltages are color-coded below. (b) Potential shape of the double-well potential along the *z*-axis for motional coupling of two identical ions. This potential can be generated with the trap geometry shown in (a) and yields an exchange time $\tau_{\mathrm{ex}} = 64$ ms at an axial trap frequency $\omega_z = 2\pi \cdot 100$ kHz.

Figure 2. Simplified schematic overview of the experimental layout. The trap can (red) is placed in the homogeneous region of the superconducting magnet. It is supported and cooled by a cryomechanical structure made of OFHC and titanium (green). This structure is supported and shielded by a radiation shield mostly made from aluminium (yellow). The vacuum chamber is continuously pumped by two turbomolecular pumps. Laser beams are introduced from the left side, whereas the imaging system and wiring is on the right side of the picture.

a spatial homogeneity $\Delta B/B < 0.3 \cdot 10^{-6}$ in a $1 \, \mathrm{cm}^3$ volume, less than $4 \cdot 10^{-5}$ over the trap stacks' extent (about 20 cm) and a temporal stability of $(\Delta B/B)(1/\Delta t) < 4 \cdot 10^{-9}/\mathrm{h}$.

3.2. Cryo-mechanical setup

An overview of the vacuum system is shown in figure 2. A horizontal bore magnet was chosen in order to be mechanically compatible with the BASE CERN setup.

The trap and wiring system form a separate cryogenic system independent from the temperature of the superconducting magnet. This allows for maintenance and upgrades on the experiment while maintaining the carefully shimmed magnetic field. All materials used in the magnet have an extremely low magnetic permeability to keep the field as homogeneous as possible. The main cold stage is cooled by the second stage of a two-stage Gifford-McMahon cryocooler equipped with a helium gas heat exchanger for vibration isolation (*ColdEdge Techologies SRDK-415 ULV UHV*) between the cold head and experiment. Our group measured an identical cooler to have vibration amplitudes

below 25 nm at the cold plate. Homemade flexible braids made from oxygen free high conductivity copper (OFHC) further reduce vibrations transmitted to the cold temperature stages and allow for thermal contraction in the apparatus. An aluminium radiation shield is thermally anchored to the first cooling stage of the cryocooler. It is mechanically fixed to the magnet using a titanium structure and disc-shaped G10CR (a glass fiber filled epoxy for low temperature use) spacers with a maze structure to minimize heat leakage. The calculated conductive heat load is about two percent of the cryocooler's cooling power at 4 K, rendering it negligible. The cryogenic trap system and wiring is mounted to the radiation shield using a similar structure. To improve thermal contact, a vacuum annealed copper rod of 99.999% purity is used for thermal contact between the cooler interface and the trap system. Radiative heat transfer is suppressed using high-reflectivity aluminium foil and multi-layer insulation blankets. Convective heat transfer is minimized by pumping the vacuum system to less than 10^{-7} mbar with two turbomolecular pumps before cooling down. With this system, we achieve temperatures of around 5 K near the trap.
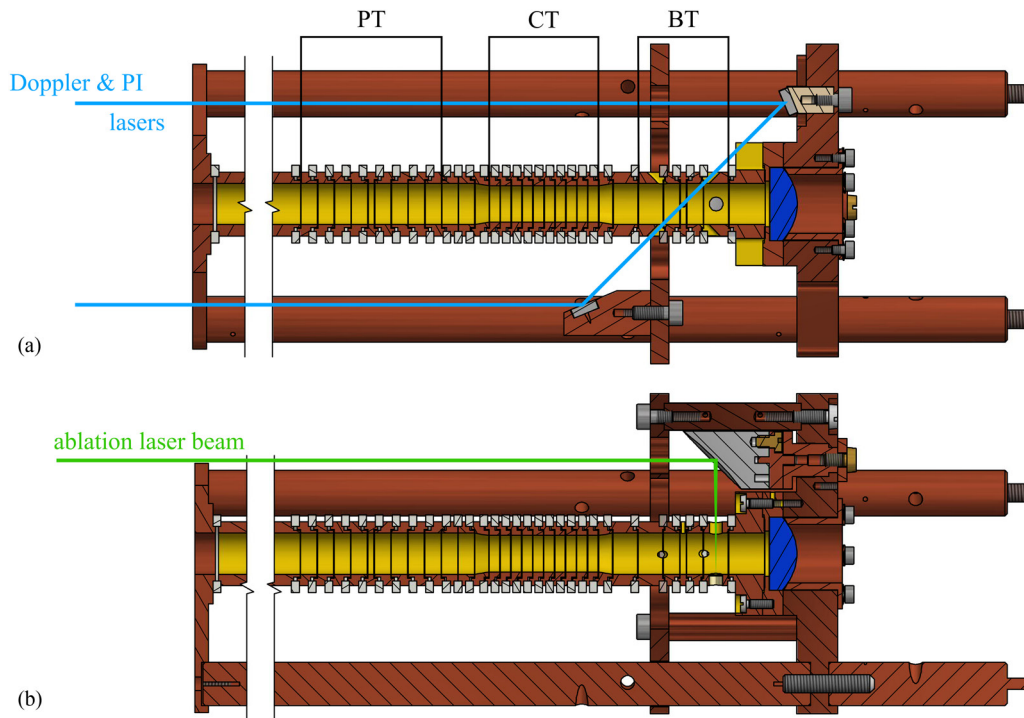
Figure 3. Trap stack and laser layout. PT: precision trap. CT: coupling trap. BT: beryllium trap. The inner trap diameter is 8 mm for the CT and 9 mm for the other traps. (a) shows the UV laser beam path that crosses the trap axis at a 45° angle and is directed out of the apparatus for beam position monitoring. (b) shows the ablation laser beam path which runs in a plane perpendicular to the plane in (a). The beam is introduced collimated and is focused by an off-axis parabolic mirror (grey) onto a beryllium disc to produce a plume of atoms.

Laser beam access is realized using custom in-vacuum mirrors to direct the beam through and out of the vacuum system. All laser beam adjustment is done outside of the vacuum chamber on a dedicated platform.

3.3. Penning trap system

The current trap system (see figure 3) consists of three cylindrical Penning traps with open endcaps located in a cylindrical OFHC 'trap can'. In order to reach the extreme high vacuum (XHV) regime necessary to prevent antiproton annihilation, the trap can be hermetically sealed to form its own cryopumped vacuum system [21]. The trap stack is comprised of a 'beryllium trap', a coupling trap and a precision trap. Extra space for additional traps, such as a proton source trap, is currently reserved with a dummy electrode. All trap electrodes are precision-machined from OFHC copper and gold-plated to prevent oxidation and minimize surface charge effects. Electrodes are separated by sapphire rings that also ensure concentric alignment of the assembly.

The beryllium trap (BT) is a compensated and orthogonal five-electrode Penning trap with laser access and loading capabilities. Single pulses from a 532 nm laser are tightly focused onto a solid beryllium target embedded in an endcap electrode using an in-vacuum off-axis parabolic (OAP) mirror to produce beryllium atoms and ions. Laser beams for photoionization, cooling and repumping are introduced using custom in-vacuum mirrors and at an angle of 45° with respect to the trap axis to allow coupling to all motional modes. The laser

beam is guided out of the vacuum chamber along a parallel path to facilitate adjustment of the beam and allow for beam position monitoring. A custom-made aspheric lens (numerical aperture NA = 0.25) collects fluorescence light, which is focused and directed onto either an EMCCD camera (*Andor iXon 885*) or a photomultiplier tube (*Hamamatsu H8259-01*) for state detection using a lens outside of the vacuum system.

The coupling trap (CT) is a stack of ten equally sized electrodes that allows for applying a double-well potential suitable for coupling the axial motional modes of two ions. For the first demonstration of the direct motional coupling of two beryllium ions in a double-well potential, we will use a trap geometry with an inner diameter of 8 mm, an inter-ion distance of $d_0 = 1$ mm and $\omega_0/(2\pi) = 100$ kHz, resulting in an exchange time $\tau_{ex} \approx 64$ ms and a coupling rate $\Omega_{ex} \approx 25$ s^{-1}.

The precision trap (PT) is a compensated, orthogonal five-electrode trap [15] that can be used for high-precision radio-frequency spectroscopy of protons. All endcap electrodes are segmented into multiple segments to allow for adiabatic transport between traps. Traps are connected with transport electrodes and the segments between the coupling electrodes and the other traps are tapered. In the context of radio-frequency Paul traps, high-fidelity transport of trapped-ion qubit essentially without affecting the temperature has been demonstrated [22], even through complicated junctions [23]. Since the axial degree of motion of the Penning trap is purely electrostatic, we expect transport along that axis to not be too different from transport along the axis of a linear Paul trap. Note that adiabatic transport is already employed in multi-trap methods for *g*-factor measurements [5, 24].
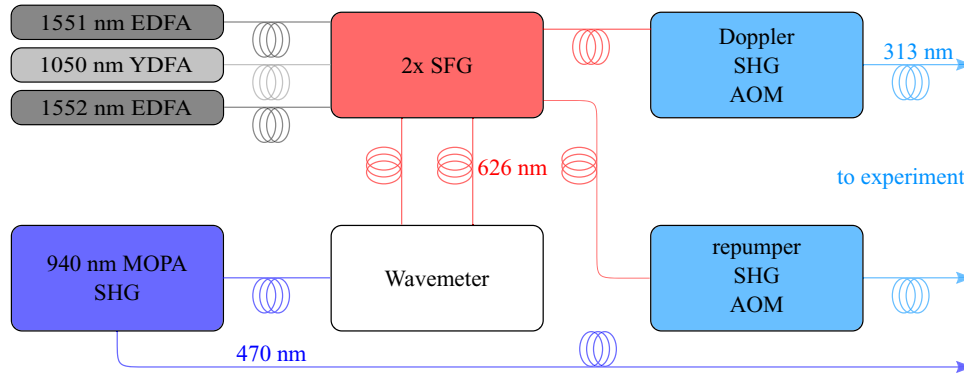
Figure 4. Schematic layout of the laser systems. The fiber amplifiers are located in a rack, while each of the other rectangular boxes in this picture represents an optical module based on aluminium breadboards of 60 cm by 60 cm size. These modules are stackable and interconnected by optical fibers. Acousto-optic modulators (AOMs) are used for intensity stabilization.

Trap voltages are supplied by a homebuilt voltage source [25] and amplifiers (*APEX PA98*). They are connected to the electrodes using low-pass filters on all three temperature stages to reduce noise and ensure thermalization of the lines. The DC voltage source used is capable of a 50 MHz update rate and limited by low-pass filters with a total cut-off frequency of 3.1 kHz outside the vacuum chamber and on the cryogenic stages. Additional coaxial lines allow for axial excitation using an endcap electrode and radial excitation using a segmented correction electrode. The system is prepared to be upgraded with image current detection systems consisting of tank circuits and ultra-low noise amplifiers to enable resistive cooling and motional frequency measurements on protons [26].

3.4. Laser systems

The laser setup is shown in figure 4. It is comprised of an ablation laser for ablation of atoms and ions, a photoionization (PI) laser for resonantly enhanced photoionization in neutral ^{9}Be, a Doppler cooling and a repumping laser.

The PI laser adresses the $\left|^1S_0, \, m_J = 0\right\rangle \rightarrow \left|^1P_1, \, m_J = 0\right\rangle$ transition near 235 nm. The Doppler and repumper lasers are tuned to the $\left|^2S_{\frac{1}{2}}, \, m_J = \frac{1}{2}, \, m_I = \frac{3}{2}\right\rangle \rightarrow \left|^2P_{\frac{3}{2}}, \, m_J = \frac{3}{2}, \, m_I = \frac{3}{2}\right\rangle$ and $\left|^2S_{\frac{1}{2}}, \, m_J = -\frac{1}{2}, \, m_I = \frac{3}{2}\right\rangle \rightarrow \left|^2P_{\frac{3}{2}}, \, m_J = \frac{1}{2}, \, m_I = \frac{3}{2}\right\rangle$ transitions, both close to 313 nm. The ablation laser is a commercial ns-pulsed, frequency doubled Nd:YAG laser near 532 nm (*Continuum Minilite*). The photoionization laser is a 940 nm master oscillator power amplfifier (MOPA) system (*TOPTICA TA pro*) that is frequency-quadrupled in two doubling stages following [27–29]. The Doppler and repumping laser beams are generated by sum frequency generation (SFG) and subsequent second harmonic generation (SHG) using the output of fiber laser systems with an ytterbium doped fiber amplifier (YDFA) close to 1050 nm and two erbium doped fiber amplifiers (EDFA) close to 1550 nm (*NKT Photonics Koheras Adjustik & Boostik*), also following the general layout of [27, 28], using the cavities described in [29]. The 313 nm laser light and the intermediate 470 nm light for the 235 nm source are guided from an optical table to a laser platform near the experiment using polarization-maintaining photonic crystal fibers (*NKT LMA-PM-10*, prepared as described in [30, 31]). The final frequency doubling stage 470 nm $\rightarrow$ 235 nm, the ablation laser source and beam shaping optics are located on that same platform. See figure 4 for a schematic layout of the laser setup. All laser sources but the ablation laser are frequency stabilised by a wavelength meter (*High Finesse WSU-2*) that is referenced to a calibrated HeNe laser source. We measured the accuracy of the wavemeter stabilisation to be better than 2 MHz over a six-hour period by beating a 626 nm laser with another one that was locked on an iodine reference via frequency modulation (FM) spectroscopy.
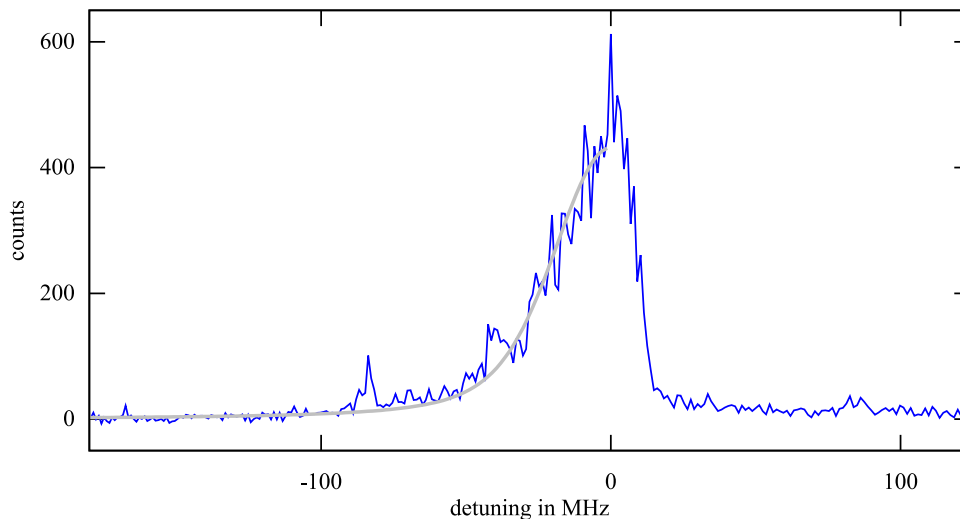
4. Results

4.1. Trap loading

Figure 5(a) shows the fluorescence image of a cloud of ^{9}Be$^+$ ions loaded by applying single pulses of the ablation laser with energies of around 500 µJ, using an axial trap frequency $\nu_z \approx 550$ kHz. The ablation laser focus diameter on the beryllium target is estimated to be on the order of 60 µm. Exact determination of the waist diameter is difficult because the laser has a multimode profile and focussing with a parabolic mirror highly depends on beam quality. Direct creation of ions by ablation from a metallic target has been reported before [32, 33]. We found that pulse energies of 40–80 µJ are sufficient to load the trap reliably. This corresponds to a peak intensity of about 0.5 to 1 GW cm^{-2} at the beryllium target's position. Below a threshold of about 30 , no loading is observed.

The loading is insensitive to photoionization laser power (or absence thereof). The reason for the insensitivity to the photoionization laser is of concern since ions produced directly by the ablation laser are expected to have much larger magnetron radii than ions that are produced in the trap center. To detect and cool the ions, we shine in laser light with a frequency close to $\nu_0 = 957.466\,784$ THz to drive the closed cycling transition $\left|^2S_{\frac{1}{2}}, \, m_J = \frac{1}{2}, \, m_I = \frac{3}{2}\right\rangle \rightarrow \left|^2P_{\frac{3}{2}}, \, m_J = \frac{3}{2}, \, m_I = \frac{3}{2}\right\rangle$. We observe a strong fluorescence signal on the EMCCD detector after loading the trap. Figures 5(b) and (c) show images of a large cloud of ions and a single ion after optimization of the imaging system. When continuously laser-cooled, clouds can be trapped for days.
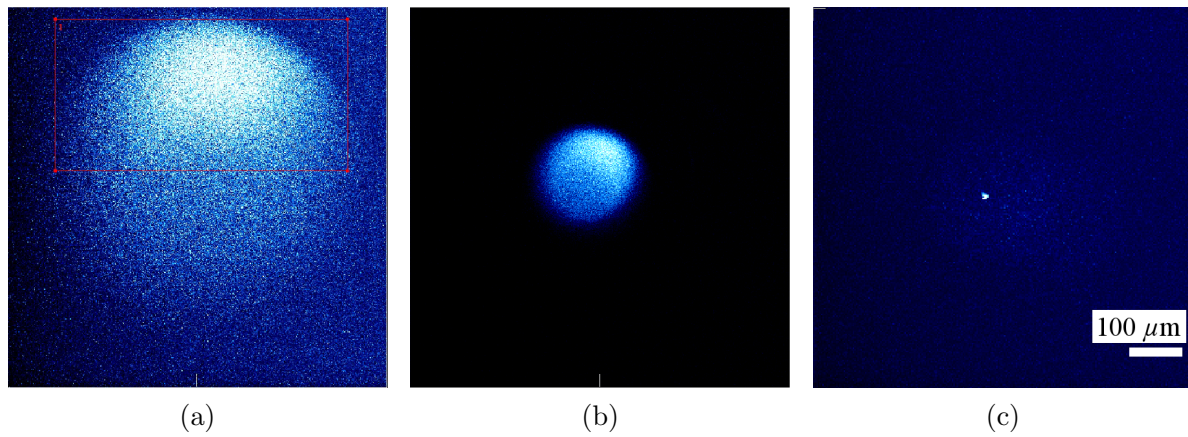
Figure 5. Fluorescence images of ^{9}Be$^+$ clouds illuminated with a near-resonant Doppler laser. (a) First trapped cloud with unoptimised imaging system. (b) Large cloud with optimised imaging system. The imaged cloud is larger than can be seen here due to clipping on apertures along the imaging path. The inhomogeneity of the brightness is due to laser beam alignment. (c) A single ion. All pictures use the same length scale, but different intensity scaling. The white bar in (c) is 100 μm long.

Figure 6. Background corrected fluorescence signal of a frequency scan with a cloud of ions (blue) and fitted Voigt profile (grey). Scattering processes on the blue-detuned side of the resonance heat the ions, resulting in an asymmetric lineshape.

4.2. Demonstration of doppler cooling

Effective laser cooling in a Penning trap is complicated by the metastable nature of the magnetron motion [34, 35]. The negative energy associated with the magnetron motion makes it hard to cool all three motional modes at the same time. When referring to 'cooling' the magnetron motion, we mean reducing its quantum number, reducing the magnetron radius and hence putting energy into the mode rather than removing it. In contrast to many other experiments, we use a single laser beam that has an inclination of 45° with respect to the trap axis, so it interacts with all motional modes.

Upon ramping the cooling laser to the red-detuned side of the resonance, we observe a distinctive change in the fluorescence spectrum over time. Directly after loading, the fluorescence is unaffected by the laser frequency over a tuning range of 1 GHz to the red of the resonance. Assuming Doppler broadening, we estimate a temperature in excess of 1000 K. Initial cooling after loading the trap takes several minutes, while subsequent recooling, e.g. after deliberate excitation,

happens on the order of seconds or faster. After cooling with a beam slightly displaced from the geometric trap centre, a clear resonance, as shown in figure 6, with a width (FWHM) of 47 MHz can be extracted from fitting a Voigt profile [36] to the red-detuned side of the spectrum. Heating processes lead to a sharp drop of fluorescence on the blue-detuned side of the resonance frequency.

Considering that the natural linewidth of the transition is 19.6 MHz [37], we deconvolve the Voigt profile with the corresponding Lorentzian lineshape, and derive a Gaussian FWHM of $\Delta\nu_D = 35.5$ MHz. Due to the noisy data, this number should be treated as an estimate of the order of magnitude rather than an accurate value. The Gaussian linewidth has contributions from saturation broadening, finite beam waist effects [38] and Doppler broadening. We neglect saturation broadening, as a low-power beam was used. We cannot reliably infer the amount of broadening due to finite beam size due to lack of information about the cloud's rotation frequency. Hence, we attribute the full Gaussian linewidth to
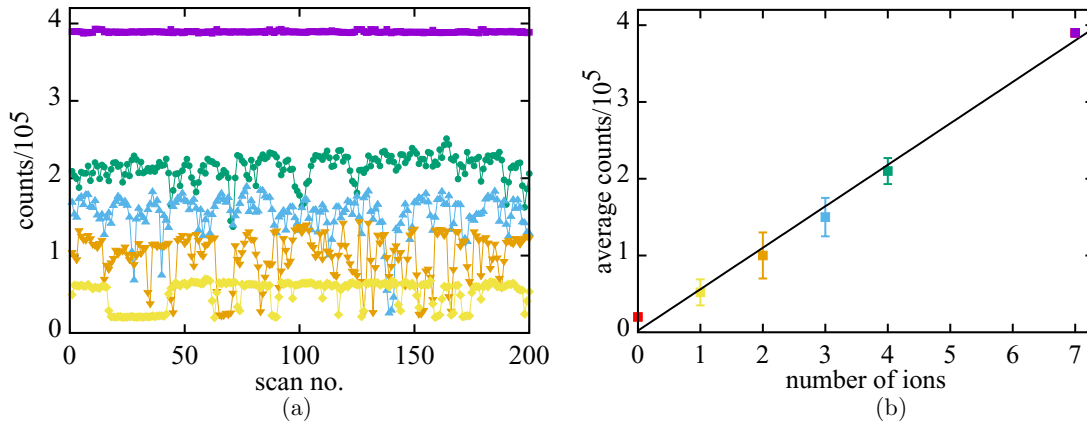
Figure 7. (a) Five time-resolved signals of individual clouds using the same trap and laser parameters. Each data point was acquired with an exposure time of 0.5 s. Stepwise decrease of the signal is visible as well as different count levels for each cloud. (b) shows the average of each measurement in (a) plotted over the inferred number of ions with a linear fit to the data points. The red point indicates the measurement background with no ions in the trap.

Doppler broadening to derive an upper temperature limit of 24 mK using [39]

$$T \leqslant \frac{(\Delta\nu_D)^2 mc^2}{8\nu_0^2 k_B \cdot \ln 2}. \tag{4}$$

The Doppler limit for the cooling transition used is 0.5 mK, hence further optimization of the cooling parameters, such as beam pointing, should allow to further decrease the temperature of the particle. By moving the laser beam away from the trap center, an intensity gradient over the radial extent of the ion's trajectory is created that allows to cool all three modes simultaneously [34, 35]. We also realized cooling of all three modes by applying a red-detuned laser to cool the axial and cyclotron modes efficiently and simultaneously irradiating a sideband drive with frequency $\nu_z + \nu_-$ (where ν_z is the axial and ν_- the magnetron frequency) to couple the two modes, thus creating a steady state in which all motional modes are cooled [40]. While clouds appeared smaller when applying sideband excitations, the temperature of the cloud was higher than in the measurement above.

4.3. Reduction of particle number

With our current loading scheme, we usually trap a large cloud of ions. Since we plan on using single ^{9}Be$^+$ ions for motional coupling and subsequent steps, we need to reduce the number of particles. Towards that end, we trap a cloud with a high negative voltage on the ring electrode of around -80 V. We then decrease the voltage by a factor of 10 to remove the most energetic particles from the trap. After some precooling, we ramp the voltage back to the original value to get a tight confinement of the remaining cloud. We then apply a voltage sequence on the electrodes to adiabatically split the ion cloud and discard a part of it. The remaining cloud is recooled subsequently. After a few of these splitting cycles, we end up with a small cloud. On numerous attempts (see figure 7), we found a smallest increment in the fluorescence signal which we attribute to a single ion. Figure 7(b) shows a linear relation between the number of ions and counts on the EMCCD

camera of 5.4×10^4 counts per ion using an exposure time of 0.5 s and an overall gain of 78 (electron multiplier gain and preamplifier of the camera). For small numbers of ions, the signal shows occasional drops in the level of fluorescence. We ascribe these to ions jumping to a higher magnetron orbit because of radiation-pressure-gradient changes induced by residual laser-beam position fluctuations. We are examining the possibility of adding an axial laser cooling beam counter-propagating with the direction of fluorescence detection, combined with mode-coupling to address the radial degrees of freedom, which should eliminate this issue.

5. Prospects and discussion

Now that the trapping infrastructure and several essential steps such as loading, cooling, and detection have been implemented successfully, we pursue the goal of demonstrating motional coupling of two individual ions in separate potential wells in a Penning trap for the first time. Since it is crucial for the coupling scheme that the axial trap frequencies are equal, our first goal is to demonstrate coupling between two ^{9}Be$^+$ ions in a symmetric potential. In addition, we are currently testing a proton source trap that will allow proton loading without blocking on-axis access to the trap. Moreover, we are setting up the associated electronics for work with protons, such as detection tank circuits and amplifiers [26].

Furthermore, we are working towards sub-Doppler cooling of ^{9}Be$^+$ in a Penning trap. While sideband cooling in a Penning trap has been demonstrated [41], the used ^{40}Ca$^+$ ions are amenable to direct sideband cooling using a single laser, as an optical qubit transition is used. For ^{9}Be$^+$, a Raman process is needed to interact with the motional modes on the single quantum level. Towards that end, the ground state hyperfine splitting must be bridged using two phase-coherent lasers with a frequency difference of around 140 GHz. This frequency gap is too large to be closed using acousto-optic modulators, as it is common to do in low-field applications. We have recently demonstrated the use of a pulsed laser [42] to drive motional

sideband transitions in $^9\text{Be}^+$ [43], an approach which can bridge this big qubit splitting.

On longer timescales, miniaturisation of the coupling trap using established techniques of microfabrication is pursued in order to increase the coupling rate. Together with ground-state cooling, manipulation of the motional states is in reach as well as quantum logic spectroscopy, potentially short-ening the preparation time of single antiprotons with spin state detection fidelity of $>98\%$ by more than two orders of magnitude [15].

Precision experiments in Penning traps usually utilize the Brown–Gabrielse invariance theorem [44] to determine the free cyclotron frequency ν_c of the particle of interest. In preci-sion studies on the p.p.b.-level and below, energy dependent systematic shifts of the eigen-frequencies of the three Penning trap modes need to be characterized and corrected. These shifts arise from trap imperfections due to non-linear terms in the trapping potential, inhomogeneities of the magnetic field, image charge and relativistic shifts, and have been summa-rized in [20, 45]. Of leading concern are shifts of the modi-fied cyclotron frequency $\nu_+(E_+, E_-, E_z)$. Here, ν_+-shifts, imposed by the weakly bound axial oscillator, constitute a dominant source of systematic uncertainty. The shift imposed by a non-vanishing magnetic bottle term B_2 of a slightly inho-mogeneous magnetic field is given by

$$\frac{\Delta\nu_+}{\nu_+} = \frac{1}{4\pi^2 m \nu_z^2} \cdot \frac{B_2}{B_0} \cdot E_z. \qquad (5)$$

For protons at a typical axial frequency $\nu_z = 650$ kHz in a magnetic field of $B_0 = 2$ T [5, 24], the fractional systematic ν_+-shift is

$$\frac{\Delta\nu_+}{\nu_+} = 2.5 \cdot 10^{-10} \cdot B_2 \cdot T_z, \qquad (6)$$

where T_z is the axial temperature of the particle. For example in non-compensated g-factor experiments B_2 is typically in a range between 0.2 T m^{-2} and 4 T m^{-2}, while $T_z \approx 10$ K [5, 24]. Depending on the chosen frequency measurement method, the $\Delta\nu_+(B_2, T_z)$-scaling can induce a dominant sys-tematic error [24]. With the axial temperature achieved in this work, and by imprinting it to the axial mode of a co-trapped antiproton in advance to a cyclotron frequency measurement, the related cyclotron frequency shift would be suppressed to a level of <20 ppt.

The axial energy exchange between an antiproton and a laser cooled Be-ion is expected to take about 60 ms. Using a sideband pulse [46], the axial energy can be translated to cyclotron mode energy, achieving $T_+ = (\nu_+/\nu_z)T_z \approx 2$ K with the trap parameters currently used. Using this scheme, a single antiproton at $T_z < 0.1$ K, and therefore a particle with a spin-state identification fidelity $>95\%$ [9], could be prepared in an effective coupling time of about 2 s. Compared to recent BASE antiproton magnetic moment measurements, this would reduce the effective ν_+-mode temperature by about a factor of 5, and the coupling time to thermalize the antiproton by more than a factor of 100. This advance would eliminate the domi-nant time-consuming step of the measurement sequence, will

enable measurements at significantly improved sampling rate and substantially lower systematic error [5, 24].

We expect that with a single particle, the axial temperature can be reduced to the Doppler limit, a factor of 40 lower [47]. This will considerably improve the performance of future magnetic moment experiments.

6. Conclusion

We have designed and commissioned a novel cryogenic Penning trap system for $^9\text{Be}^+$ ions. We have successfully demonstrated ablation loading, Doppler cooling, and reduc-tion of the number of ions down to a single particle which has been detected unambiguously. We have outlined the next steps towards motional coupling and sympathetic cooling of two ions that can be generalized to arbitrary charged ions. We anticipate a high impact of the sympathetic cooling scheme on precision measurements in Penning traps, such as *q/m*- or *g*-factor measurements on antiprotons and protons, molecular ions or other systems that are not amenable for direct laser cooling.

ORCID iDs

M Niemann ● https://orcid.org/0000-0002-5267-8142
T Meiners ● https://orcid.org/0000-0002-8356-8587
J Mielke ● https://orcid.org/0000-0003-0865-9398
S Ulmer ● https://orcid.org/0000-0002-4185-4147
C Ospelkaus ● https://orcid.org/0000-0002-4170-2936

References

[1] Lüders G 1957 Proof of the TCP theorem *Ann. Phys.* **2** 1–15
[2] Greenberg O W 2002 *cpt* violation implies violation of Lorentz invariance *Phys. Rev. Lett.* **89** 231602
[3] Smorra C *et al* 2018 350-fold improved measurement of the antiproton magnetic moment using a multi-trap method *Hyperfine Interact.* **239** 47
[4] Higuchi T *et al* 2018 Progress towards an improved comparison of the proton-to-antiproton charge-to-mass ratios *Hyperfine Interact.* **239** 27
[5] Schneider G *et al* 2017 Double-trap measurement of the proton magnetic moment at 0.3 parts per billion precision *Science* **358** 1081–4
[6] Ulmer S *et al* 2015 High-precision comparison of the antiproton-to-proton charge-to-mass ratio *Nature* **524** 196–9
[7] Häffner H, Beier T, Djekić S, Hermanspahn N, Kluge H-J, Quint W, Stahl S, Verdú J, Valenzuela T and Werth G

2003 Double Penning trap technique for precise g factor determinations in highly charged ions *Eur. Phys. J.* D **22** 163–82

[8] Borchert M *et al* 2019 Measurement of ultralow heating rates of a single antiproton in a cryogenic Penning trap *Phys. Rev. Lett.* **122** 043201

[9] Smorra C *et al* 2017 Observation of individual spin quantum transitions of a single antiproton *Phys. Lett.* B **769** 1–6

[10] Heinzen D J and Wineland D J 1990 Quantum-limited cooling and detection of radio-frequency oscillations by laser-cooled ions *Phys. Rev.* A **42** 2977

[11] Wineland D J, Monroe C R, Itano W M, Leibfried D, King B E and Meekhof D M 1998 Experimental issues in coherent quantum-state manipulation of trapped atomic ions *J. Res. NIST* **103** 259

[12] Brown K R, Ospelkaus C, Colombe Y, Wilson A C, Leibfried D and Wineland D J 2011 Coupled quantized mechanical oscillators *Nature* **471** 196–9

[13] Harlander M, Lechner R, Brownnutt M, Blatt R and Hansel W 2011 Trapped-ion antennae for the transmission of quantum information *Nature* **471** 200–3

[14] Niemann M, Paschke A-G, Dubielzig T, Ulmer S and Ospelkaus C 2013 CPT test with (anti)proton magnetic moments based on quantum logic cooling and readout *CPT and Lorentz Symmetry* (Singapore: World Scientific) pp 41–4

[15] Smorra C *et al* 2015 BASE–the Baryon antibaryon symmetry experiment *Eur. Phys. J. Spec. Top.* **224** 1–54

[16] Gutiérrez M J *et al* 2019 The trapsensor facility: an open-ring 7 tesla Penning trap for laser-based precision experiments *New J. Phys.* **21** 023023

[17] Bohman M *et al* 2018 Sympathetic cooling of protons and antiprotons with a common endcap Penning trap *J. Mod. Opt.* **65** 568–76

[18] Larson D J, Bergquist J C, Bollinger J J, Itano W M and Wineland D J 1986 Sympathetic cooling of trapped ions: a laser-cooled two-species nonneutral ion plasma *Phys. Rev. Lett.* **57** 70–3

[19] Gruber L, Holder J P, Steiger J, Beck B R, DeWitt H E, Glassman J, McDonald J W, Church D A and Schneider D 2001 Evidence for highly charged ion coulomb crystallization in multicomponent strongly coupled plasmas *Phys. Rev. Lett.* **86** 636–9

[20] Brown L S and Gabrielse G 1986 Geonium theory: physics of a single electron or ion in a Penning trap *Rev. Mod. Phys.* **58** 233–311

[21] Sellner S *et al* 2017 Improved limit on the directly measured antiproton lifetime *New J. Phys.* **19** 083023

[22] Rowe M A *et al* 2002 Transport of quantum states and separation of ions in a dual RF ion trap *Quantum Inf. Comput.* **2** 257

[23] Blakestad R B, Ospelkaus C, VanDevender A P, Amini J M, Britton J, Leibfried D and Wineland D J 2009 High-fidelity transport of trapped-ion qubits through an x-junction trap array *Phys. Rev. Lett.* **102** 153002

[24] Smorra C *et al* 2017 A parts-per-billion measurement of the antiproton magnetic moment *Nature* **550** 371–4

[25] Bowler R, Warring U, Britton J W, Sawyer B C and Amini J 2013 Arbitrary waveform generator for quantum information processing with trapped ions *Rev. Sci. Instrum.* **84** 033108

[26] Nagahama H *et al* 2016 Highly sensitive superconducting circuits at ∼700 kHz with tunable quality factors for image-current detection of single trapped antiprotons *Rev. Sci. Instrum.* **87** 113305

[27] Wilson A C, Ospelkaus C, VanDevender A P, Mlynek J A, Brown K R, Leibfried D and Wineland D J 2011 A 750 mW, continuous-wave, solid-state laser source at 313 nm for cooling and manipulating trapped $^9Be^+$ ions *Appl. Phys.* B **105** 741–8

[28] Lo H-Y, Alonso J, Kienzler D, Keitch B C, de Clercq L E, Negnevitsky V and Home J P 2014 All-solid-state continuous-wave laser systems for ionization, cooling and quantum state manipulation of beryllium ions *Appl. Phys.* B **114** 17–25

[29] Hannig S, Mielke J, Fenske J A, Misera M, Beev N, Ospelkaus C and Schmidt P O 2018 A highly stable monolithic enhancement cavity for second harmonic generation in the ultraviolet *Rev. Sci. Instrum.* **89** 013106

[30] Colombe Y, Slichter D H, Wilson A C, Leibfried D and Wineland D J 2014 Single-mode optical fiber for high-power, low-loss UV transmission *Opt. Express* **22** 19783–93

[31] Marciniak C D, Ball H B, Hung A T H and Biercuk M J 2017 Towards fully commercial, UV-compatible fiber patch cords *Opt. Express* **25** 15643–61

[32] Chichkov B N, Momma C, Nolte S, von Alvensleben F and Tünnermann A 1996 Femtosecond, picosecond and nanosecond laser ablation of solids *Appl. Phys.* A **63** 109–15

[33] Zimmermann K, Okhapkin M V, Herrera-Sancho O A and Peik E 2012 Laser ablation loading of a radiofrequency ion trap *Appl. Phys.* B **107** 883–9

[34] Itano W M and Wineland D J 1982 Laser cooling of ions stored in harmonic and Penning traps *Phys. Rev.* A **25** 35–54

[35] Thompson R C and Papadimitriou J 2000 Simple model for the laser cooling of an ion in a Penning trap *J. Phys. B: At. Mol. Opt. Phys.* **33** 3393–405

[36] Olivero J J and Longbothum R L 1977 Empirical fits to the Voigt line width: a brief review *J. Quantum Spectrosc. Radiat. Transfer* **17** 233–6

[37] Andersen T, Jessen K A and Sørensen G 1969 Mean-life measurements of excited electronic states in neutral and ionic species of beryllium and boron *Phys. Rev.* **188** 76–81

[38] Brewer L R, Prestage J D, Bollinger J J, Itano W M, Larson D J and Wineland D J 1988 Static properties of a non-neutral $^9Be^+$ -ion plasma *Phys. Rev.* A **38** 859–73

[39] Foot C J 2005 *Atomic Physics Oxford Master Series in Atomic, Optical and Laser Physics* (Oxford: Oxford University Press)

[40] Dehmelt H G 1976 Entropy reduction by motional sideband excitation *Nature* **262** 777

[41] Goodwin J F, Stutter G, Thompson R and Segal D 2016 Resolved-sideband laser cooling in a Penning trap *Phys. Rev. Lett.* **116** 143002

[42] Hayes D, Matsukevich D N, Maunz P, Hucul D, Quraishi Q, Olmschenk S, Campbell W, Mizrahi J, Senko C and Monroe C 2010 Entanglement of atomic qubits using an optical frequency comb *Phys. Rev. Lett.* **104** 140501

[43] Paschke A-G, Zarantonello G, Hahn H, Lang T, Manzoni C, Marangoni M, Cerullo G, Morgner U and Ospelkaus C 2019 Versatile control of $^9Be^+$ ions using a spectrally tailored UV frequency comb *Phys. Rev. Lett.* **122** 123606

[44] Brown L S and Gabrielse G 1982 Precision spectroscopy of a charged particle in an imperfect Penning trap *Phys. Rev.* A **25** 2423–5

[45] Ketter J, Eronen T, Höcker M, Streubel S and Blaum K 2014 First-order perturbative calculation of the frequency-shifts caused by static cylindrically-symmetric electric and magnetic imperfections of a Penning trap *Int. J. Mass Spectrom.* **358** 1–16

[46] Cornell E A, Weisskoff R M, Boyce K R and Pritchard D E 1990 Mode coupling in a Penning trap: π pulses and a classical avoided crossing *Phys. Rev.* A **41** 312–5

[47] Sawyer B C, Britton J W and Bollinger J J 2014 Spin dephasing as a probe of mode temperature, motional state distributions, and heating rates in a 2d ion crystal *Phys. Rev.* A **89** 033408